Astron. Astrophys. 335, 431–442 (1998)

ASTRONOMY AND ASTROPHYSICS

Counterrotating galaxies formed by cosmological collapses

M. Harsoula and N. Voglis

Department of Astronomy, University of Athens, GR-157 84 Athens, Greece

Received 21 January 1998 / Accepted 16 March 1998

Abstract. We investigate numerically the possibility that dissipationless cosmological collapses can lead to the formation of counterrotating galaxies. We consider systems formed from initially small density excesses embedded in the environment of other density perturbations in an otherwise homogeneous and isotropic expanding early Universe.

We find that a central bar-like density excess, that can make bound a mass of the order of galactic mass can work as a seed able to initiate counterrotating galaxies. Such objects are formed rather naturally as a result of the partial mixing between the material in which positive angular momentum dominates with the material in which negative angular momentum dominates. The initial axial ratio of the bar-like perturbation is a control parameter in this process. Counterrotation is favored for an axial ratio ≈ 0.5. The rotational velocity profile in the relaxed state of these configurations matches to a great extent the curves given from observations, for some elliptical galaxies, presenting kinematically decoupled cores.

Performing parallel simulations of the same system by N-body and by conservative technique codes we show that the rotational velocity curve, established after the relaxation, maintains its basic features even for a Hubble time. Therefore counterrotating galaxies observed today could have been formed directly from cosmological initial conditions.

Key words: galaxies: formation – galaxies: evolution – galaxies: kinematics and dynamics

1. Introduction

A structure born from small initial density peturbations in an otherwise homogeneous and isotropic expanding Universe, acquires angular momentum from the tidal field due to other small perturbations that break the isotropy of its environment (Hoyle 1949, Peebles 1969, Doroshkevich 1970, White 1984). A reasonable question concerns the distribution of angular momentum along the radius of the relaxed object. In particular it is of interest to test whether such a distribution can be consistent with the phenomenon of counterrotation observed in galaxies. Counterrotating cores have often been observed in ellipticals, via radial velocity profiles, i.e. stellar velocity dispersion curves or line of sight velocities (e.g. Davies et al. 1983, Franx & Illingworth 1988, Bender 1988, Franx et al. 1989, Bender & Surma 1992). Generally, in recent years, it became evident that in probably up to 1/3 of luminous ellipticals the core regions are kinematically decoupled from the main bodies of the galaxies. Most of the observers suggest that a merger event can be responsible for this counterrotation and N-body simulations have shown it with demonstration of the formation of a counter rotating central disk in a merger of two gas-rich disk galaxies (Hernquist & Barnes 1991, Barnes & Hernquist 1996). Other suggestions for the creation of counterrotating systems have been made in the literature, using episodic gass infall, continuous gass infall, or a merger with a gas-rich dwarf galaxy. Although both episodic and continuous gas infall work reasonably well and produce counterrotating gas disks, a gas rich dwarf merger does not appear to be a viable mechanism to produce a massive counterrotating disk, because the timescale for this process is prohibitively long (Thakar & Ryden 1996).

An alternative scenario, in which galaxies that present counterrotation have been formed in a single collapse (Bender 1988) is also possible, as we will see below. In this case, the two counterrotating parts reflect to some extent the surviving memory of cosmological initial conditions.

In the field of small fluctuations in an otherwise homogeneous and isotropic expanding early Universe (at decoupling) consider a density excess that makes bound a mass M, i.e. destined to detach itself from the general expansion and collapse to form a galaxy. Let S be the surface surrounding this mass (Fig. 1). Inside this surface there may be several local density peaks of various mass scales smaller than M. These peaks lead to subclumps which merge during the collapse of the mass M and are at least partially dissolved. The mass M cannot be isolated. Other density perturbations of various mass scales outside S create an anisotropic environment and therefore an external tidal field exerting a torque on M. Thus the material inside S acquires angular momentum. The external torque vanishes when the mass M collapses provided that the environment still expands. Thus the total angular momentum that has been transferred to M up to this time remains constant. The distribution of the angular momentum along the radius cannot be unique. It

Send offprint requests to: M. Harsoula

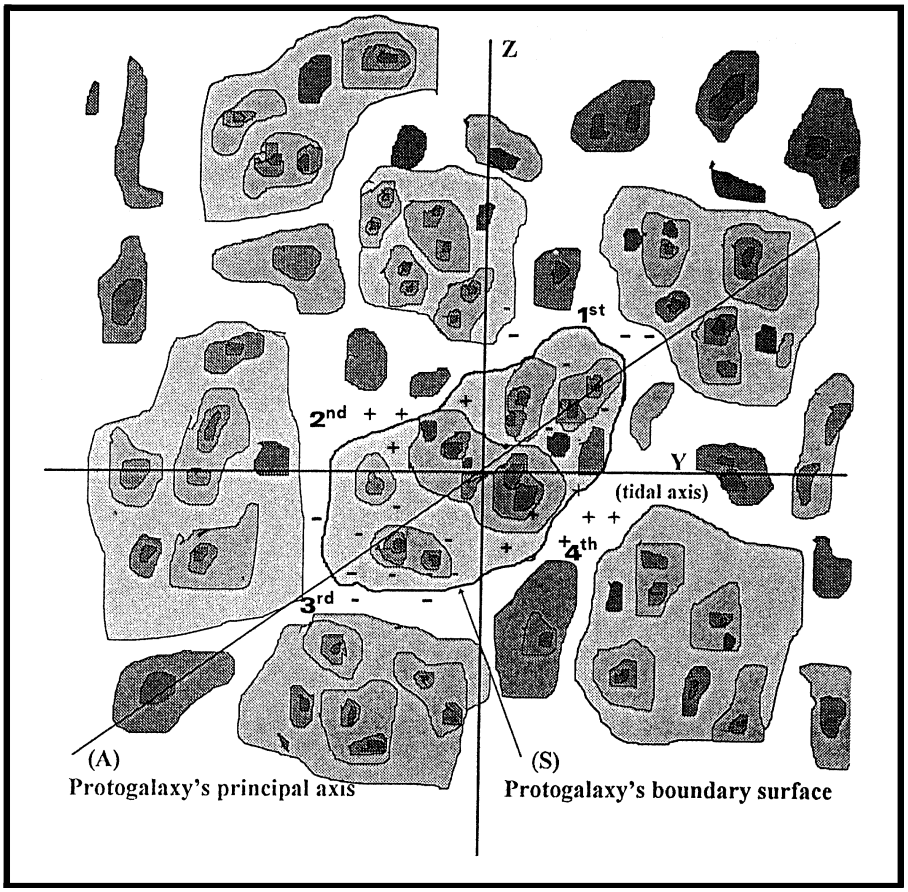

Fig. 1. A schematic representation of density excesses in a hierarchical clustering scenario. A density excess inside the surface S at decoupling exposed to the tidal field of its environment is destined to detach from the general expansion and collapse to form a rotating galaxy. Plus and minus signs indicate the sign of the tidal torque acting on individual particles.

depends on the initial position in space of the various subclumps relative to the center of mass M and the direction of the external tidal field.

This scenario can apply to any mass scale in the hierarchical clustering scenario. The most important case, however, is the galactic mass scale. For this reason, our terminology refers to galaxies.

The density perturbations in the close environment of a protogalaxy are significant for angular momentum transfer. However, angular momentum can be transferred to a protogalaxy even from the anisotropic distribution of remote matter. This has been shown in numerical simulations where the close neighbouring material is neglected and the protogalaxy is exposed to the tidal field of a large scale environment (Voglis & Hiotelis 1989).

The angular momentum grows mainly during the linear phase of evolution of the density perturbations. This growth can be given by analytical expressions up to second order in the density perturbation. It depends on the strength and on the time behaviour of the external tidal field as well as on the shape of the boundary surface of the protogalaxy and its initial density perturbation profile.

In Sect. 2 these analytical expressions are discussed. In Sect. 3 the model of initial conditions and the ability of simulating the expected growth of angular momentum are described. The results are given in Sect. 4 and show the possibility of creation of counterrotating galaxies in a cosmological collapse (primary and secondary infall). In Sect. 5 we check the stability of the rotational curves in a Hubble time by performing parallel runs by a direct N-body code and a conservative technique code. Our conclusions are summarized in Sect. 6.

2. Analytic approximations of the torque on the protogalaxy

Let $\boldsymbol{r_i}$ and $\boldsymbol{R_j}$ be the position vectors of two point masses m_i and m_j (i inside the boundary surface S and j outside S, Fig. 1). The total torque exerted on the mass inside S is: (Barnes & Efstathiou 1987, Voglis & Hiotelis 1989):

$$\boldsymbol{\Gamma} = \frac{1}{a} \sum_i \sum_j G m_i m_j \frac{\boldsymbol{x_i} \times \boldsymbol{x_j}}{\mid \boldsymbol{x_i} - \boldsymbol{x_j} \mid^3} \tag{1}$$

where a is the scale factor of the universe and $\boldsymbol{x_i} = \frac{\boldsymbol{r_i}}{a}, \boldsymbol{x_j} = \frac{\boldsymbol{R_j}}{a}$ are the comoving vectors. At an initial time, at which we define a to be equal to 1 let $\boldsymbol{q}$ be the unperturbed comoving position vector (Langrangian) of a test particle and $\boldsymbol{\delta q}$ a small displacement ($\mid \delta \boldsymbol{q} \mid \ll \mid \boldsymbol{q} \mid$) due to the presence of density perturbations. Then, before the collapse, the Zeldovich approximation is valid (Zeldovich 1970):

$$\boldsymbol{x} = \boldsymbol{q} + b\delta\boldsymbol{q} \tag{2}$$

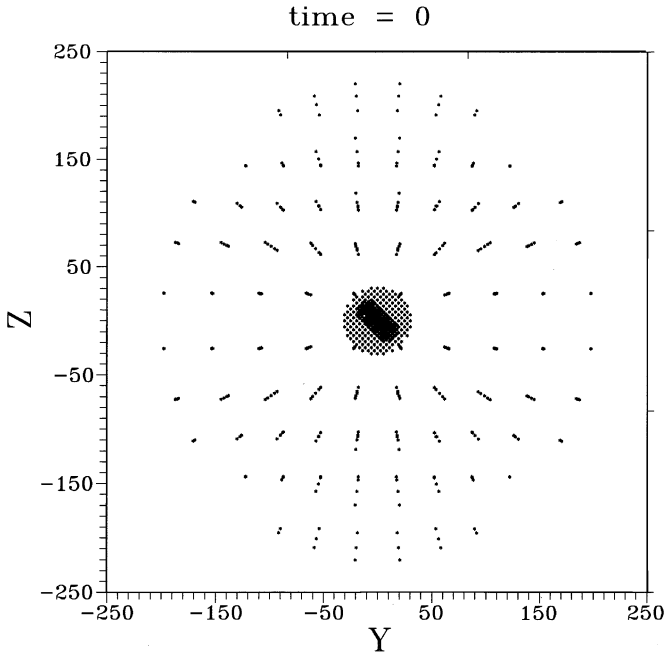

Fig. 2. The projection of the initial configuration on the Y-Z plane at a time = 0.

where b is a function of time only. For an Einstein de Sitter model, b is given by the equation:

$$b(t) \propto a(t) \propto t^{2/3} \tag{3}$$

Eq. (1) can be written, up to second order in $\delta\boldsymbol{q}$ as:

$$\boldsymbol{\Gamma} = \boldsymbol{\Gamma_0} + \boldsymbol{\Gamma_1} + \boldsymbol{\Gamma_2} \tag{4}$$

where $\boldsymbol{\Gamma_0} = \frac{1}{a}\boldsymbol{F_0}(\boldsymbol{q})$, $\boldsymbol{\Gamma_1} = \frac{b}{a}\boldsymbol{F_1}(\delta\boldsymbol{q})$, $\boldsymbol{\Gamma_2} = \frac{b^2}{a}\boldsymbol{F_2}(\delta\boldsymbol{q}^2)$ or in an Einstein de Sitter model:

$$\boldsymbol{\Gamma_0} \propto t^{-2/3}\boldsymbol{F_0}(\boldsymbol{q}) \tag{5}$$

$$\boldsymbol{\Gamma_1} \propto \boldsymbol{F_1}(\delta\boldsymbol{q}) \tag{6}$$

$$\boldsymbol{\Gamma_2} \propto t^{2/3}\boldsymbol{F_2}(\delta\boldsymbol{q}^2) \tag{7}$$

were $\boldsymbol{F_0}, \boldsymbol{F_1}, \boldsymbol{F_2}$ are functions, independent of time, of zero, first and second order in $\delta\boldsymbol{q}$, respectively. The zero order torque $\boldsymbol{\Gamma_0}$ must be zero, because it corresponds to a perfectly homogenous and isotropic universe. However, in N-body simulations it may contaminate the results, because of the finite volume V, adopted for the N-Body simulations and because of the discreteness that breaks the balance of the zero order torque from particles outside S. In our simulations presented below special care has been taken to minimize the magnitude of $\boldsymbol{\Gamma_0}$ on the level of a few percent of the $\boldsymbol{\Gamma_1}$ term. It is however worth noting that in a perturbed Universe, the very close environment can exert itself a cosmological torque $\boldsymbol{\Gamma_0}$ on the protogalaxy, but it is small and decreases faster in time than the other terms and its contribution to the growth of total angular momentum is small.

The first order torque $\boldsymbol{\Gamma_1}$ depends on the shape of the surface S and equals zero when S is spherical (Peebles, 1969). This term couples the zero-order quadrupole moment of the protogalaxy to the external first-order tidal field (White, 1984). The second order torque $\boldsymbol{\Gamma_2}$, is related to the initial density perturbation, inside and outside the boundary surface S, and becomes the leading term if S is spherical.

The angular momentum during the linear phase of expansion is given by the integral:

$$J = \int \Gamma dt \ \propto t^{1/3}F_0(\boldsymbol{q}) + tF_1(\delta\boldsymbol{q}) + t^{5/3}F_2(\delta\boldsymbol{q}^2) \tag{8}$$

The last two terms are the most important modes of the angular momentum of the protogalaxy during the expansion phase.

Another way of approximating the total torque exerted on a protogalaxy because of the anisotropy of the environment, is by the equation:

$$\Gamma \propto QI_{out} \tag{9}$$

with

$$I_{out} = \int \boldsymbol{n}\sin(2\Theta)\frac{Gdm}{R^3} \tag{10}$$

where the integration extends over the whole Universe outside S. In Eq. (10) $\boldsymbol{n}$ is the unit vector in the direction of the torque element and Θ is the angle between the position vector $\boldsymbol{R}$ of a point mass dm outside the surface S and the orientation of the major axis of the protogalaxy. The quantity Q is the quadrupole moment of the protogalaxy and it can be written as:

$$Q \propto MA^2 f(e) \tag{11}$$

where A is the length of the major axis of the protogalaxy and $f(e)$ is a function of its eccentricities.

Notice that the derivation of Eq. (10) assumes that $R >> A$. This means that the effects of the material outside S at distances R comparable to A have been neglected. The point mass dm in the integral (10) can be replaced as $dm = \rho_b[1 + s(R,\theta,\phi)].R^2\sin\theta d\theta d\phi dR$ in terms of the mean density of the Universe ρ_b and the density perturbation $s(R,\theta,\phi)$ at the position (R,θ,ϕ) outside the boundary surface S. Since an unperturbed environment does not exert any torque on the mass M of the protogalaxy, the integral I_{out} can be written as:

$$I_{out} = \int G\rho_b s(R,\theta,\phi)\boldsymbol{n}\sin(2\Theta)\sin\theta\frac{dR}{R}d\theta d\phi \tag{12}$$

From the expression of the integral (12) we can make two remarks.

First, this integral contains a logarithmic divergence as $R \to \infty$, unless the density perturbation $s(R,\theta,\phi)$ decreases with R. This means that the torque Γ in Eq. (9) is finite only because of the large scale isotropy of the Universe.

Second, when the expansion of the protogalaxy ceases and its major axis starts to decrease, the quadrupole moment of the protogalaxy does not evolve considerably in time, i.e. $Q(M, A^2, e) \approx$ constant. Then, the torque Γ evolves in time mainly through the integral I_{out}. If the environment continues to expand and the perturbations in it grow linearly, then

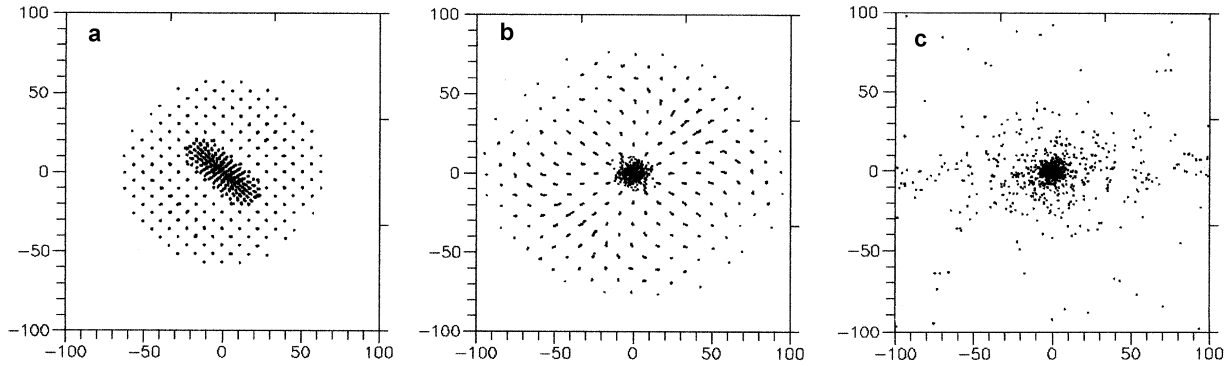

Fig. 3a–c. Three snapshots of the evolution of the G-scale, at times $t_1 = 100$ Myrs **a**, $t_2 = 200$ Myrs **b** and $t_3 = 2,000$ Myrs **c**.

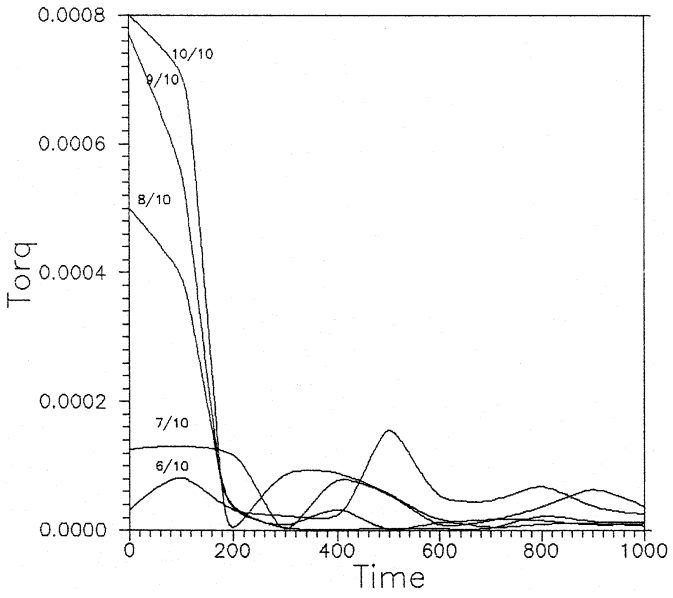

Fig. 4. The total tidal torque acting on the matter belonging to the material G1, due to the rest of the mass, as a function of time.

$\rho_b \propto \frac{1}{a^3} \propto \frac{1}{t^2}$ and $s \propto b \propto a \propto t^{2/3}$ in Eq. (12). Therefore, the cosmological torque in Eq. (9) evolves in time as:

$$\Gamma \propto \frac{1}{a^2} \propto t^{-4/3} \tag{13}$$

For large t the torque tends to vanish and the galaxy is left with a net amount of angular momentum.

If a galaxy is formed as a member of a rich cluster the behaviour of the torque may be different, depending on several parameters through the integral I_{out}, e.g. the position of the galaxy in the cluster, the density of the cluster etc. Important phenomena can occur in this case, such as tidal stripping, merging of galaxies, changes of morphology, warping etc., which will not be discussed here.

3. Initial conditions

A special N-body model of initial conditions, that is efficient for studying the problem of angular momentum transfer to a protogalaxy from its environment with relatively low computational cost, has been proposed by Voglis & Hiotelis (1989) and Voglis et al. (1991). The advantage of this model is that we can obtain the time behavior of the torque exerted on a protogalaxy from the environment, which is consistent with the analysis in the previous section. Furthermore, we can investigate the response of the system under different values of a relatively small number of parameters such as the time scales of collapse and the geometry of the boundary surface as regards the protogalaxy, or the initial strength and the time evolution of the tidal field as regards the environment. The basic idea is to study the simultaneous evolution and the interaction of two very different mass scales in the Universe. For a better understanding we give here a description of the most essential points of the model.

a)Unperturbed configuration:
We define two different mass scales: the Galactic scale (G-scale) and the environment scale (E-scale). The evolution of these two scales is followed simoultaneously, in a single run. The G-scale is a sphere, resolved into $N_1 = 2176$ particles, in a cubic grid arrangement. The total mass of the G-scale is $2M_u$, where M_u is the mass unit equal to the typical galactic mass. This scale is surrounded by the E-scale, which is a spherical part of the Universe homocentric to the G-scale, containing a much larger amount of mass. The E-scale is resolved into $N_2 = 664$ particles with one galactic mass for every particle, arranged also in a cubic grid. Eight particles in the central region of this grid have been removed and replaced by the G-scale. The grid steps either of the G-scale or of the E-scale are so arranged that the total energy in both scales is zero. (As a consequence the distances of all particles increase as $t^{2/3}$ simulating an Einstein de Sitter Universe).

Inside the sphere of the G-scale, we define an homocentric prolate spheroidal surface surrounding a total mass of $1M_u$ approximately. We call G1 the material inside this prolate surface and G2 the rest of the material inside the G-scale.

The major axis of the prolate spheroid lies on the YZ plane and defines an angle $\Theta = -45^o$ with the Y-axis. In this configuration if we calculate the total torque on G1 due to the E-scale only, we find that a non cosmological, zero order torque Γ_0, dominates. This torque is due to the discreteness of the E-scale, which is composed of a small number of heavy particles. The torque due to every one of these particles is of zero order and

should be balanced by an opposite torque of another particle in a symmetric position. In order to obtain this balance of zero order torques, we deform the grid of the E-scale, by the formula:

$$\boldsymbol{q}_{i,new} = \boldsymbol{q}_{i,old}[1 + c_1(1 + c_2 \cos\omega_i + \cos 4\omega_i)] \quad (14)$$

where $\boldsymbol{q}_i$ is the position vector in the XYZ frame of the i particle belonging to the E-scale. The angle ω_i is the angle between $\boldsymbol{q_{i,old}}$ and the Y axis. For suitable values of c_1, c_2, this non cosmological torque Γ_0 is suppressed to an almost zero value. The new E-scale behaves as an isotropic environment with respect to the prolate spheroid. This is an artificial isotropy, i.e. pseudo-isotropy.

The essential of the above "unperturbed configuration" is that if we impose a small density perturbation to the E-scale we obtain a behaviour of the torque on the material G1 that agrees in the linear phase of evolution with the analytic predictions given in Sect. 2 (Eqs. 4–7).

b) Perturbed configuration:
The prolate spheroidal surface considered in 3a is defined by the equation:

$$\frac{q_1^2 + q_3^2}{a^2} + \frac{q_2^2}{b^2} = \lambda^2 = 1 \quad (15)$$

where q_1 is parallel to the X-axis and q_2 makes an angle Θ with the Y-axis. The major axis b of the prolate spheroid is approximately equal to the unperturbed radius of the G-scale. The ratio $\kappa = a/b$ is a free parameter. By definition the material G1 corresponds to particles of G-scale inside the prolate surface i.e. particles whose coordinates (q_1, q_2, q_3) give $\lambda \leq 1$. This part is made bound by imposing on it a density perturbation having an amplitude S_1 and a shallow mean radial profile ($\approx \frac{1}{r^{0.2}}$). This is obtained by locating the particles of G1 in phase space according to the Zeldovich approximation:

$$\boldsymbol{r} = a_1(\boldsymbol{q} - b_1\boldsymbol{Y}) \quad (16)$$

$$\dot{\boldsymbol{r}} = \dot{a_1}(\boldsymbol{q} - b_1\boldsymbol{Y}) - a_1\dot{b_1}\boldsymbol{Y} \quad (17)$$

where the scale factor of the Universe (normalised to be $a = 1$ at decoupling i.e. at a redshift Z = 1000) has a value $a = a_1$ when the N-body run starts. The vector $\boldsymbol{Y}$ is given by the equation:

$$\boldsymbol{Y} = \frac{S_1\boldsymbol{q}}{(1 + \frac{\lambda}{\lambda_0})^n} \quad (18)$$

with $n = 0.2$ and $\lambda_0 = 0.1$. Then, the density perturbation $\delta\rho/\rho$ becomes maximum near the center ($\lambda \approx 0$) of the prolate spheroid and at decoupling it is $\delta\rho/\rho = S_1\nabla Y \approx 3S_1$.

The material G2 (i.e. the rest of the G-scale) is also perturbed in a similar way but with a different amplitude $S_2 < S_1$. This difference of the amplitudes between G1 and G2, leads to different time evolutions between the two parts of the G-scale, i.e. G1 has a typical time of expansion and collapse shorter than the typical time of G2. The shallow mean radial profile is used in order to make more sharp the distinction between these two time scales.

The particles of the E-scale are also perturbed using the Zeldovich approximation, (equations similar to 16, 17), where the components of the perturbing vector $\boldsymbol{Y}$ is given by the formulae:

$$Y_1 = (S_4 + 2S_3\cos^2\omega).q_1 \quad (19)$$

$$Y_2 = (S_4 - 2S_3\sin^2\omega).q_2 \quad (20)$$

$$Y_3 = (S_4 + 2S_3\cos^2\omega).q_3 \quad (21)$$

where q_1, q_2, q_3 are the components of the position vector $\boldsymbol{q}_{new}$ of the individual E-scale particles. The angle ω is the angle between the Y-axis and $\boldsymbol{q}_{new}$. S_4 corresponds to radial displacements and S_3 to transverse displacements. The cosmological torque on G1 or G2 depends directly on the parameter S_3. This is because the anisotropy of the E-scale is introduced by the terms in (19–21) containing ω which all have an amplitude proportional to S_3. The values of S_3, S_4 are smaller than S_1.

Such a perturbation of the E-scale initiates the formation of two clusters of galaxies with their centers in symmetric positions along the Y-axis and creates a tidal field with stronger forces along the Y-axis (tidal axis). The control of both the strength and the time evolution of this tidal field is obtained by tuning properly the parameters S_3 and S_4.

A remark which is important for couterrotation is the following: Let the prolate spheroidal shape of G1 have a quadrupole moment Q1 and a major axis A1 on the YZ plane oriented at an angle Θ with respect to the tidal axis. The distribution of mass in G2 has a different quadrupole moment Q2 with a major axis A2 also on the YZ plane, but oriented at an angle $\Theta + 90^o$ relative to the Y-axis, i.e. A2 is perpendicular to A1. As a consequence the corresponding total tidal torques on G1 and G2 due to the E-scale have opposite signs. This geometry can in principle initiate counterrotating parts in the object under formation depending also on the level of mixing of the materials belonging initially to G1 and G2. (A similar correlation between the quadrupole moments Q1, Q2 could be realised even if the G-scale is initially spheroidal instead of spherical. Thus the main feature of the above initial conditions working as a seed for counterrotation is the central bar-like perturbation).

In our model, for fixed values of S_1, S_2 and S_4, the distribution of angular momentum along the radius in the relaxed galaxy depends mainly on three parameters. First, it depends on the axial ratio $\kappa = a/b$ of G1 and second on the initial strength of the tidal field controlled by the parameter S_3.

A distribution of angular momentum established shortly after the period of violent relaxation, i.e. after the first few dynamical times, can be altered by a slow secular evolution of the galaxy. In order to compare the corresponding rotational velocity curves with the ones observed today in galaxies we have to follow the evolution for times comparable to the age of the Universe.

The scaling units of length and time are defined in Voglis & Hiotelis (1989). Namely, if the unit of mass is $M_u = 10^{12}$ solar masses, the unit of length is $r_u = 1.5\beta$ kpc and the unit of time is $t_u = 0.86\beta^{\frac{3}{2}}$ Myr. The velocity unit is $v_u = 1677\beta^{-\frac{1}{2}}$ km/sec. In these expressions β is a rescaling parameter depending on the precise values of the amplitude of pertubations (that

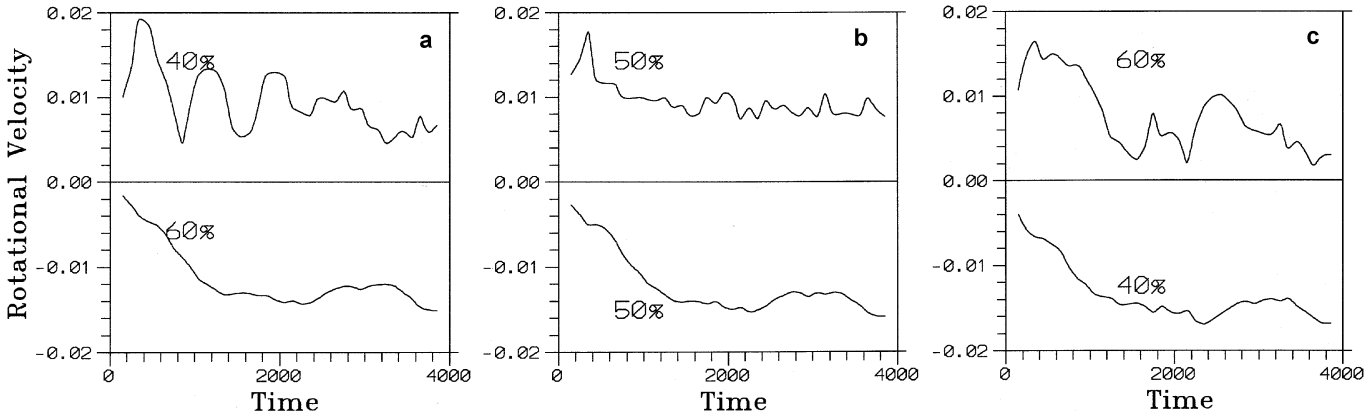

Fig. 5a–c. Positive curves give the time evolution of the mean rotational velocity of the inner 40% **a**, 50% **b** and 60% **c** of the bound mass. Negative curves give the same but for the remainder of the bound mass.

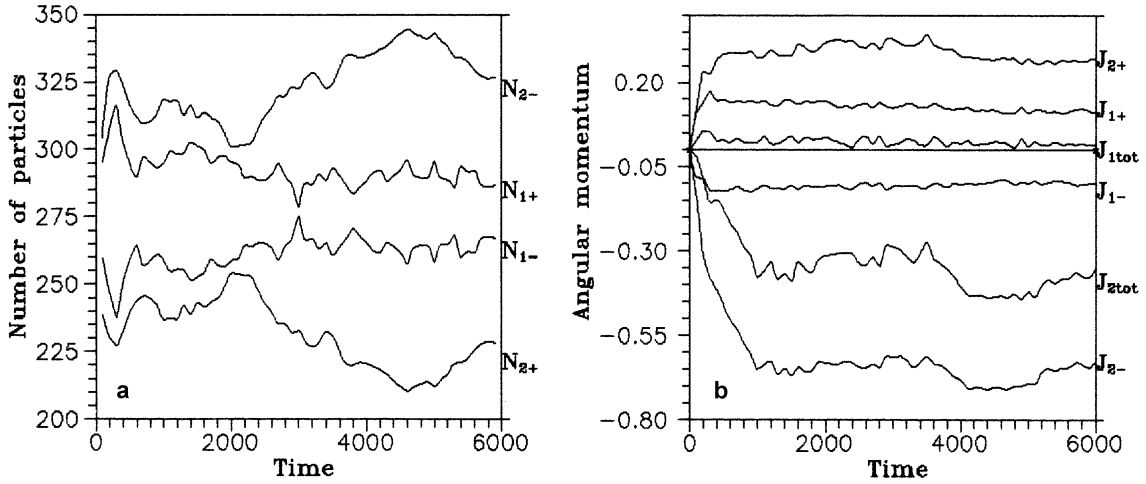

Fig. 6. **a** time evolution of the number of particles having positive and negative angular momenta in the inner 50%(N_{1+}, N_{1-}) and respectively in the outer 50%(N_{2+}, N_{2-}) of the bound matter. **b** time evolution of positive and negative component of the angular momentum (J_{1+}, J_{1-}), (J_{2+}, J_{2-}) corresponding to the four parts of mass described in **a**. J_{1tot} and J_{2tot} are the total angular momentum of the inner 50% and the outer 50% of the bound mass respectively.

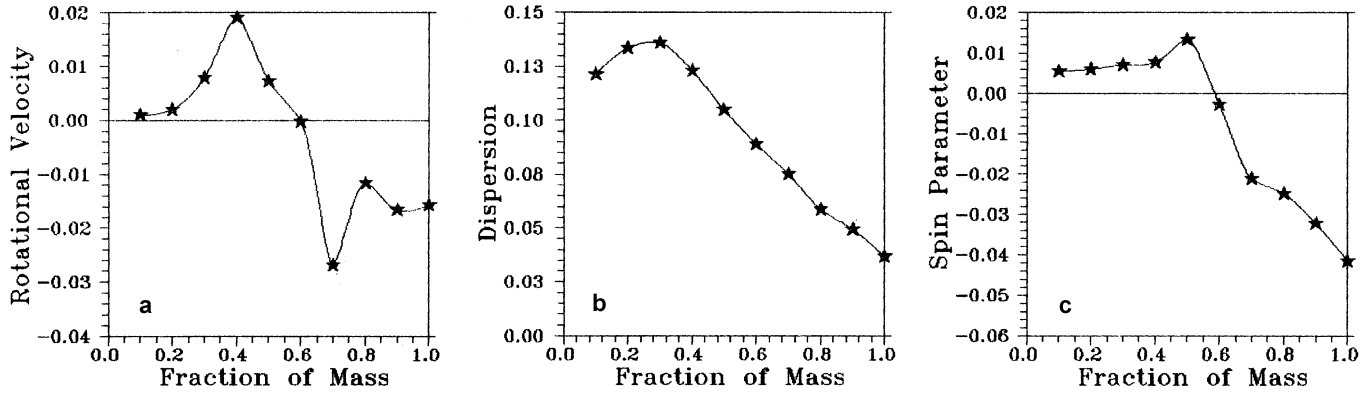

Fig. 7a–c. Rotational velocity curve **a**, dispersion velocity curve **b**, and spin parameter **c** as a function of the cumulative bound mass.

determine the epoch of galaxy formation and hence the virial velocity in the dissipationless collapse and relaxation). If in an experiment a mass $M = 0.5M_u$ is virialized in a radius $R = x$, the virial velocity (estimated by $v^2_{virial} = \frac{M}{2R}v^2_u$) is $v_{virial} = \frac{1}{2\sqrt{x}}v_u = 1677(4x\beta)^{-\frac{1}{2}}$ km/sec. Therefore if x is known β could be evaluated from the velocity dispersion observed in galaxies today.

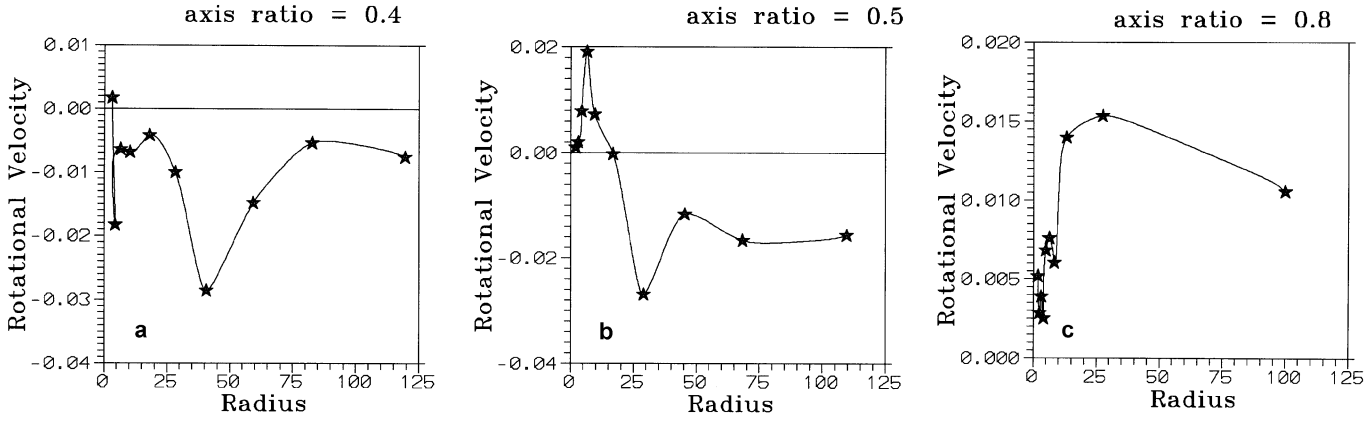

Fig. 8a–c. Rotational velocity curves as a function of radius for the experiments E4-55 **a**, E5-55 **b** and E8-55 **c** at a $time = 6000$ Myrs.

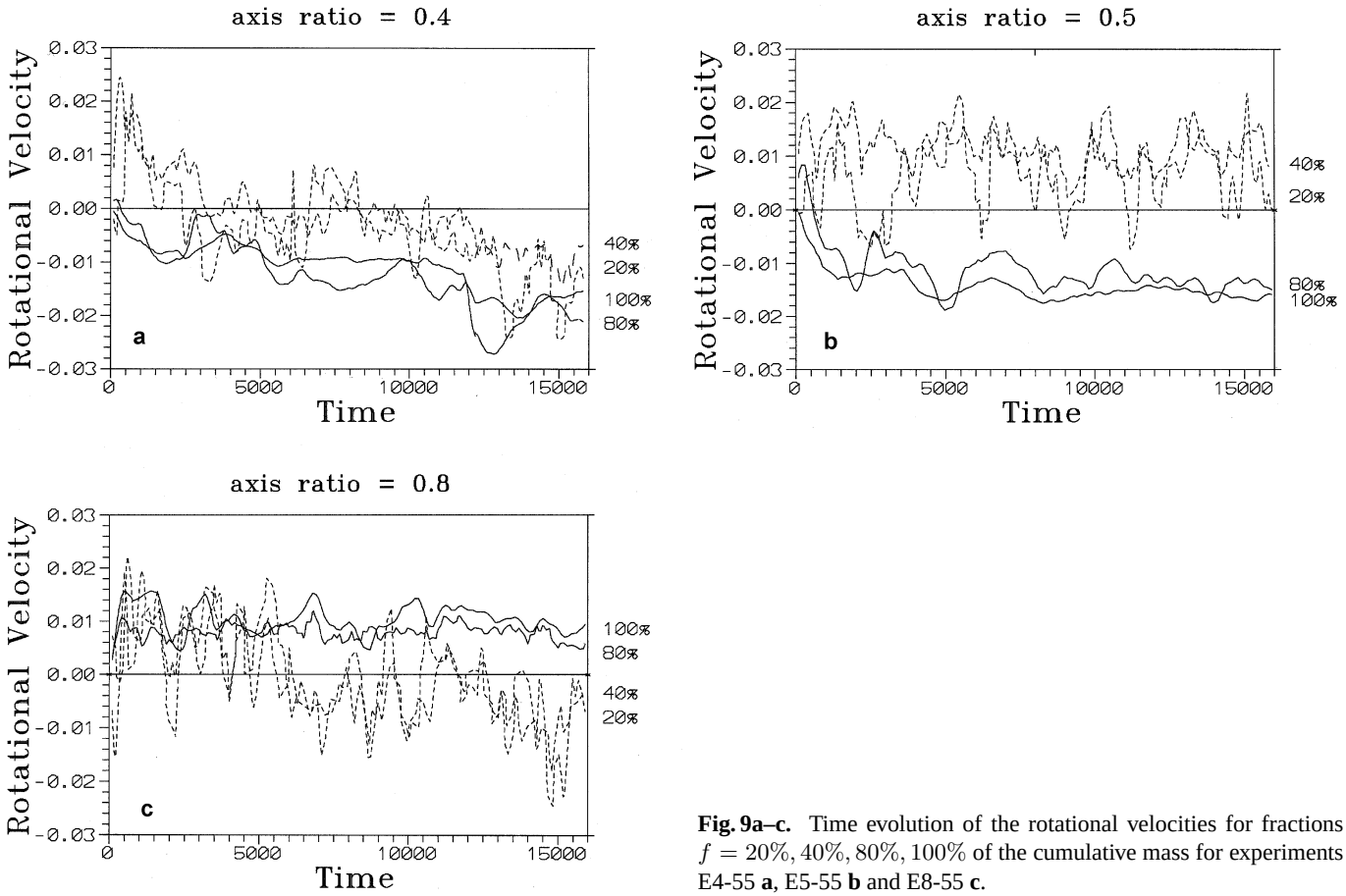

Fig. 9a–c. Time evolution of the rotational velocities for fractions $f = 20\%, 40\%, 80\%, 100\%$ of the cumulative mass for experiments E4-55 **a**, E5-55 **b** and E8-55 **c**.

In Fig. 2 the overall projection of initial configuration is shown on the YZ plane at the time = 0, (scale factor = $a = a_1 = 25$) when the N-body calculations start.

The G-scale in Fig. 2 is the dark circle at the center with the two density perturbation levels corresponding to G1 (dark spheroid at the center) and G2 (all the rest of the G-scale).

Three snapshots of the evolution of G-scale are shown in Figs. 3a–c at times $t_1 = 100$, $t_2 = 200$, and $t_3 = 2000$ respectively as a typical example of our experiments. At t_3 the bound material is almost relaxed and separated from the unbound particles of the G-scale. The E-scale continues to expand and the perturbations in it still evolve linearly.

An idea of how the torque on the material G1 evolves can be given as follows. Let us consider a radius r_f from the center which contains a fraction f of the mass belonging to G1 only. The total tidal torque acting on this fraction of mass, due to all the rest of the mass, is shown in Fig. 4. The numbers above the various curves indicate the respective values of f. For the inner radii r_f ($f < \frac{6}{10}$) the distribution of the matter inside r_f is almost spherical. As a consequence the dominant term of the torque is $\Gamma_2 \propto t^{2/3}$ and the total torque initially increases. For

$f > \frac{6}{10}$ the term $\Gamma_1 (= constant)$ of the torque (Eq. 6) is the dominant term and the total torque on this part is roughly constant except for a small decreasing component Γ_0 due mainly to the very close environment of G1 (material G2) as noted in Sect. 2. Fig. 4 can be interpreted as a verification of the ability of the model to simulate the behaviour of cosmological torque, which is the result of small differences of competing gravitational interactions.

When the expansion of G_1 ceases at about $t = 200$ the torque drops quickly to much smaller values and finally vanishes.

4. Results

4.1. Detecting counterrotation

In the results presented below (selected among a good number of numerical experiments) the values of S_1, S_2, S_4 are fixed at $0.03,\ 0.0,\ 0.0$ respectively.

Counterrotation is detected as follows: We define a radius r_f from the center of mass of the bound system on the Y-Z plane containing a particular fraction f of the bound mass. If J_{fx} is the total angular momentum of this mass (oriented along the X-axis i.e. the axis of rotation) and $I_{fyz} = \Sigma m_i (y_i^2 + z_i^2)^{1/2}$ is the first moment, then we find a mean velocity of rotation of this mass as:

$$V_1 = \frac{J_{fx}}{I_{fyz}} \tag{22}$$

A similar process is followed to find the mean velocity V_2 of the rest of the bound mass. Counterrotation is recognised if V_1 and V_2 have opposite signs.

In Fig. 5 such an example is given for the experiment with $\kappa = 0.5$ and $S_3 = 0.0055$ (experiment E5-55). The time evolution of V_1 (positive) and V_2 (negative) is shown for $f = 40\%$ in (a), $f = 50\%$ in (b) and $f = 60\%$ in (c). From this figure we see the tendency of the difference $V_1 - V_2$ to be maximum at $f \approx 50\%$. Thus we can say that in about 50% of the inner mass the positive angular momentum dominates while in the rest of the mass the negative angular momentum dominates.

Let N_{1+}, N_{1-} be the number of particles with positive and negative angular momentum respectively that at any given time belong to the inner 50% of the bound matter and N_{2+}, N_{2-} the corresponding number of particles in the outer part. The time evolution of these four parameters is shown in Fig. 6a. Counterrotation is due to the fact that at all times $N_{1+} > N_{1-}$ and $N_{2+} < N_{2-}$.

The corresponding values of angular momentum denoted by J_{1+}, J_{1-}, J_{2+} and J_{2-} evolve in time as in Fig. 6b. They start from zero and grow up to a final value that remains almost constant beyond a time of about 1000. The algebraic sum of J_{1+} and J_{1-} gives the total angular momentum J_{1tot} in the inner part which remains positive. On the other hand, J_{2-} and J_{2+} give a sum J_{2tot} in the outer part which remains negative (Fig. 6b). As we will see below this distribution of angular momentum is permanent even for a Hubble time.

For a more detailed investigation of the rotation properties of the system we define 10 cylinders parallel to the rotation axis so that 10% of the bound mass is contained between sucessive cylinders. Then the rotational velocity curve is found by applying again the formula (22) but f now counts these cylinders (f = 1,2,...,10).

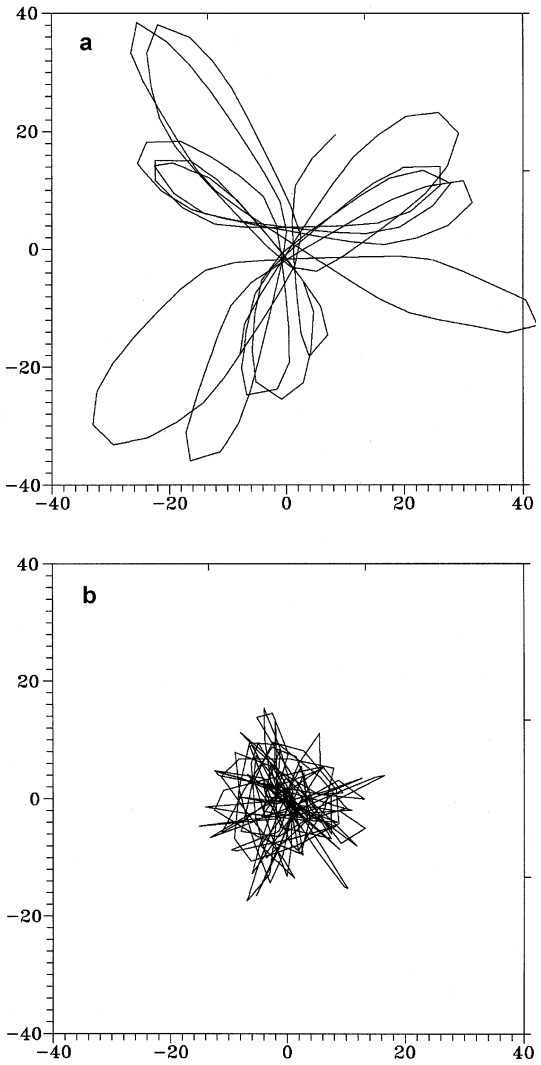

Fig. 10. **a** Projection on the Y-Z plane of the orbit of a particle carrying negative angular momentum until $time = 6800$ Myrs, **b** Its subsequent evolution until $time = 16000$ Myrs **b**.

In Fig. 7a the rotation curve of this experiment is shown as a function of the cumulative mass M from the center at a time $t = 6000$ when the whole configuration has relaxed. The horizontal coordinate of a star in this figure corresponds to a fraction $f/10$ of the cumulative mass and the vertical coordinate gives the mean value of the rotational velocity of the particles between the cylinders $f-1$ and f. The transition to the negative rotational velocity occurs at about 50% of the cumulative mass.

In Fig. 7b the dispersion velocity curve along the X-axis $\sigma =< V_x^2 >^{1/2}$ is presented as a function of the cumulative mass. The dispersion velocity σ at the half mass in Fig. 7b is about 0.1, about five times larger than the maximum rotational velocity in Fig. 7a. This ratio is comparable to the corresponding ratio in observational data (see e.g. Franx et al. 1989).

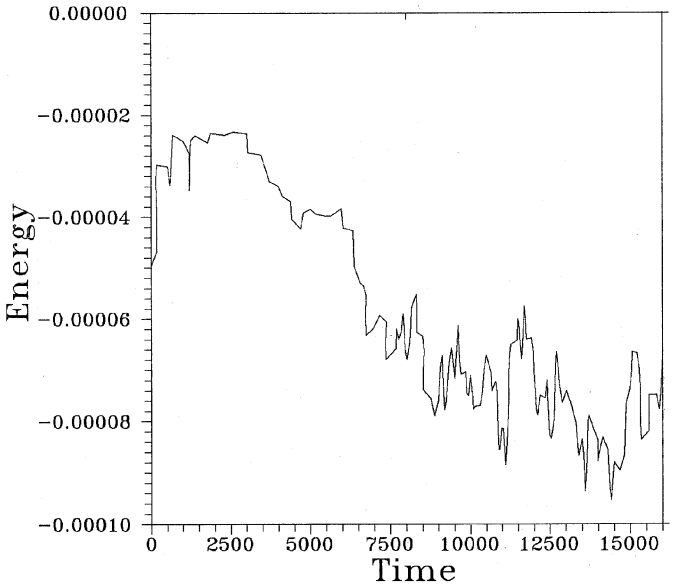

Fig. 11. Time evolution of the energy of the particle whose orbit is shown in Fig. 10.

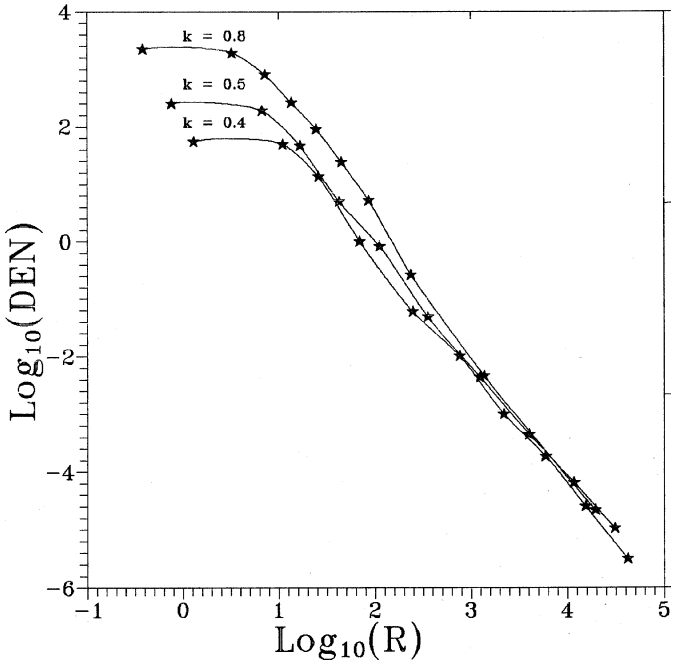

Fig. 12. Surface density profiles of the experiments E4-55, E5-55 and E8-55 ($\kappa = 0.4, 0.5, 0.8$ respectively).

In Fig. 7c counterrotation is shown in terms of the spin parameter λ (Peebles 1969):

$$\lambda = \frac{J \mid E \mid^{1/2}}{G.M^{5/2}} \tag{23}$$

where the angular momentum J, the bounding energy E, and the mass M are measured as cumulative quantities along the cylinders on the Y-Z plane defined above. In this diagram the parameter λ is plotted versus the cumulative mass M from the center. We see again that the transition occurs at about 50% of the mass where the curve $\lambda(M)$ has a maximum. At the end of the system it approaches the typical mean value of $\lambda = 0.05$ found in other cosmological simulations (Barnes & Efstathiou 1987, Quinn et al. 1986, Voglis & Hiotelis 1989, Voglis et al. 1991).

The experiment described above shows that in principle cosmological initial conditions can lead to direct formation of counterrotating galaxies. However this effect depends on the values of the parameters which can alter the ratio between positive and negative components of angular momentum as well as the ratio between tightly and loosely bound matter. In the next section we examine the role of the initial axial ratio κ of the bar-like perturbation which seems to be important.

4.2. Counterrotation and the initial axial ratio of the bar

The appearance of counterrotation depends on the relative size of the two components of angular momentum (positive and negative) and on whether or not they can be well mixed. In our model a decisive role on this aspect is played by the initial axial ratio of the central bar, .i.e. the material G1. We present below the results for $\kappa = 0.4$ (experiment E4-55) and $\kappa = 0.8$ (experiment E8-55) and we compare them with the results in the previous section (experiment E5-55). In Fig. 8 the rotation curves of these three experiments are presented at a time $t = 6000$. Stars in this figure indicate the radius containing a fraction of cumulative mass as in Fig. 7. In Fig. 8a (E4-55)the rotation curve is negative almost all along the radius except of a small counterrotating core of about 10% of the bound mass. This is in contrast with Fig. 8c (E8-55) where the rotation curve is positive all along the radius, while in Fig. 8b (E5-55) the rotation curve corresponds to the counterrotating galaxy analysed in the previous section. These impressive differences between the three cases are only due to the initial axial ratio κ of the bar (more precisely to the length of the minor axis of the spheroid since the major axis is fixed). Thus by changing only the parameter κ in our model we have obtained three quite different rotation curves.

We can understand this behaviour as follows. For smaller axial ratio, e.g. $\kappa = 0.4$ the material in G1 is less and acquires smaller amount of positive net angular momentum. Therefore, in the relaxed galaxy the central region is more sensitive in changing the mean rotation from positive to negative as particles in radial orbits and negative rotation, pass through the center. For an intermediate axial ratio $\kappa = 0.5$ more positive angular momentum is concentrated initially near the center, while the number of particles with radial orbits which pass through the center is smaller. Therefore, a counterrotating core can survive.

On the other hand if the axial ratio is as large as $\kappa = 0.8$ the mass in G1 is large and the positive angular momentum of this part dominates everywhere along the radius of the bound mass.

5. Time evolution of the rotation curves

5.1. Evolution of rotation curves in direct N-body simulations

An important question is whether a given distribution of angular momentum, established shortly after the relaxation, as in the

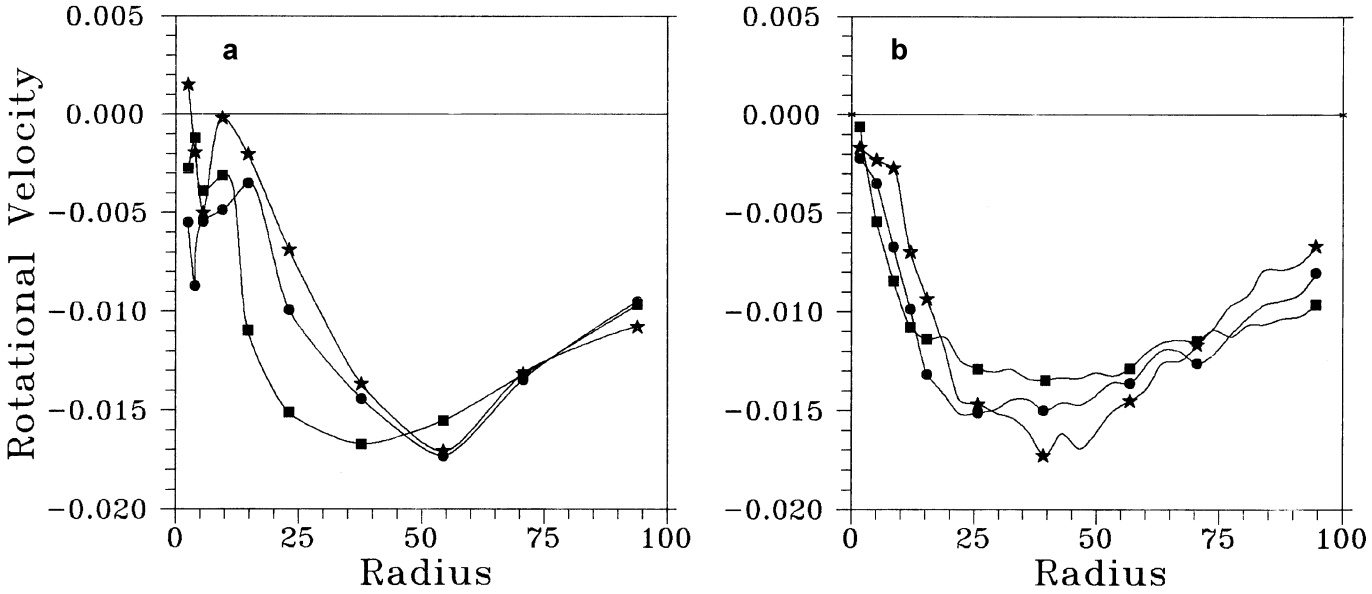

Fig. 13a and b. Experiment E4-55. **a** time averages of the rotational velocities V_f in the intervals $\Delta t_1 = (4000, 8000)$, $\Delta t_2 = (8000, 12000)$ and $\Delta t_3 = (12000, 16000)$ (curves with stars, squares and cycles respectvely) given from the N-Body code. **b** as in **a** but from the c-t code.

cases of the previous section, can survive for a Hubble time. We have extended our simulations up to the time $t = 16000$. This time is comparable to the age of the Universe if the parameter β in the scaling unit of time is close to 1.

In Fig. 9 the time evolution of the rotational velocity is given up to this time for the fractions $f = 20\%, 40\%, 80\%, 100\%$ of the cumulative mass for the three cases of Fig. 8. The total angular momentum ($f = 100\%$) in the three cases remains almost constant throughout the whole evolution, but it is negative in 9a and 9b, while it is positive in 9c.

A remarkable feature in Fig. 9a is that the inner parts ($20\%, 40\%$) have initially positive rotation until $t = 2000 - 3000$ but their rotation is inverted and remains negative until the end of the simulation (except for a short transient period from $t = 7000$ to $t = 8000$). This effect is due to the secondary infall of loosely bound particles passing through the central region. Most of these particles carry a relatively large amount of negative angular momentum which is tranferred to the central region of the galaxy. Thus, the positive rotation of this region is inverted. However, a small core at the center could preserve its positive rotation, since the pericenters of the infalling particles with considerable amount of angular momentum cannot be very small. Therefore, if counterrotating galaxies observed today are formed according to this mechanism a very small counterrotating core should be considered as a natural event.

In Fig. 9b ($\kappa = 0.5$) it is obvious that counterrotation of the inner parts survives for a time comparable to the Hubble time, whithout considerable changes.

In Fig. 9c ($\kappa = 0.8$) the inversion of rotation of the inner bound parts of the galaxy is observed again, as in Fig. 9a, but at a time $t \approx 6000$. The reason of this inversion in the inner parts is different. We have thoroughly followed sever al orbits of particles responsible for this effect in the inner parts. A number of particles moving initially in radial orbits with large apocentres and carrying negative angular momentum, are "trapped" later on in a small inner region. Fig. 10 shows a typical example of such an orbit. The projection of the orbit in the Y-Z plane until time $t = 6800$ is shown in Fig. 10a while the subsequent evolution, until time $t = 16000$ is shown in Fig. 10b. This orbit has negative angular momentum and its mean radius becomes smaller by a factor of more than 2 during the evolution. The time evolution of the energy of this particle plotted in Fig. 11 shows that the energy decreases by the same factor.

This phenomenon is related to the process of two-body relaxation which becomes important in this experiment after a time $t \approx 6000$, because the mass here is more centrally concentrated and denser than in the other experiments. The surface density of the three experiments is shown in Fig. 12 at a time $t = 6000$. The case with $\kappa = 0.8$ has a core 40 times denser than in $\kappa = 0.4$ and 10 times denser than in $\kappa = 0.5$. This is due to the initial conditions (greater fraction of tightly bound mass). Therefore in $\kappa = 0.8$ case the two-body relaxation process becomes effective earlier than in the other cases. In order to check the reliability of our results beyond a time of $t = 6000$ we perform a parallel evolution of every system beyond $t = 4000$ with a conservative technique code and compare the results.

5.2. Comparison to the results by a conservative technique code

A snapshot from each of the three previous experiments at a time $t = 4000$, where violent relaxation of the main bound part is completed, is used as initial conditions in the conservative technique code (the c-t code) designed by Allen, Palmer & Papaloizou (1990). In the c-t code Poisson's equation is solved in terms of spherical Bessel functions and spherical harmon-

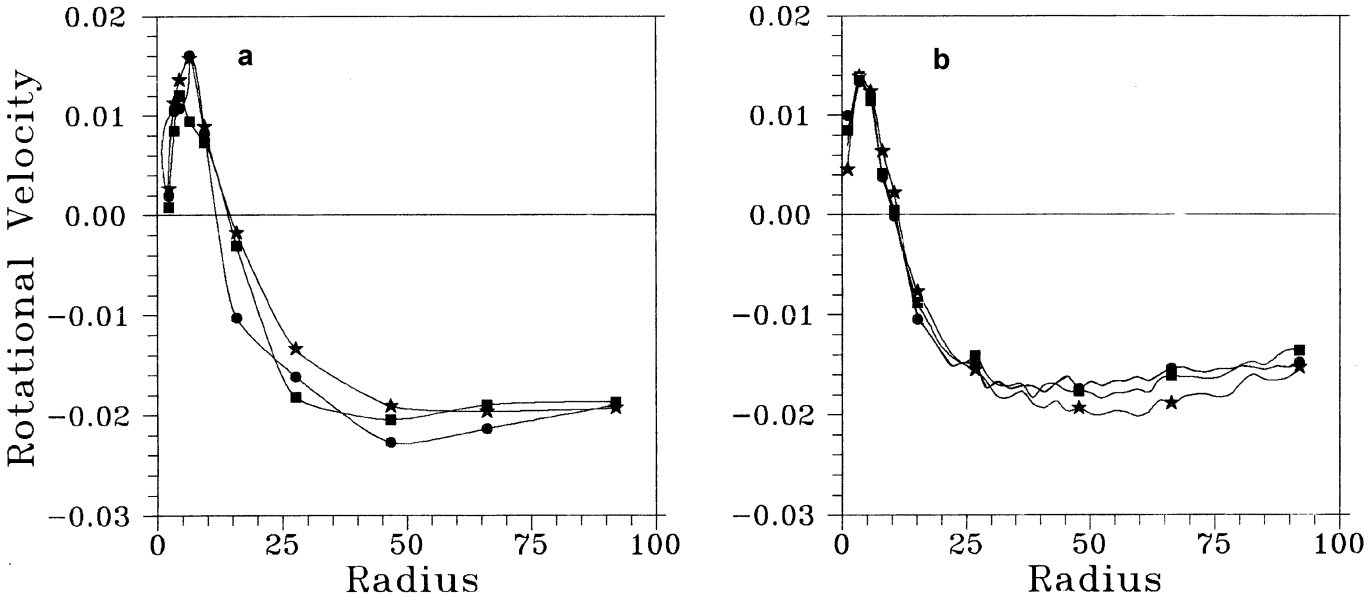

Fig. 14a and b. As in Fig. 13 for the experiment E5-55.

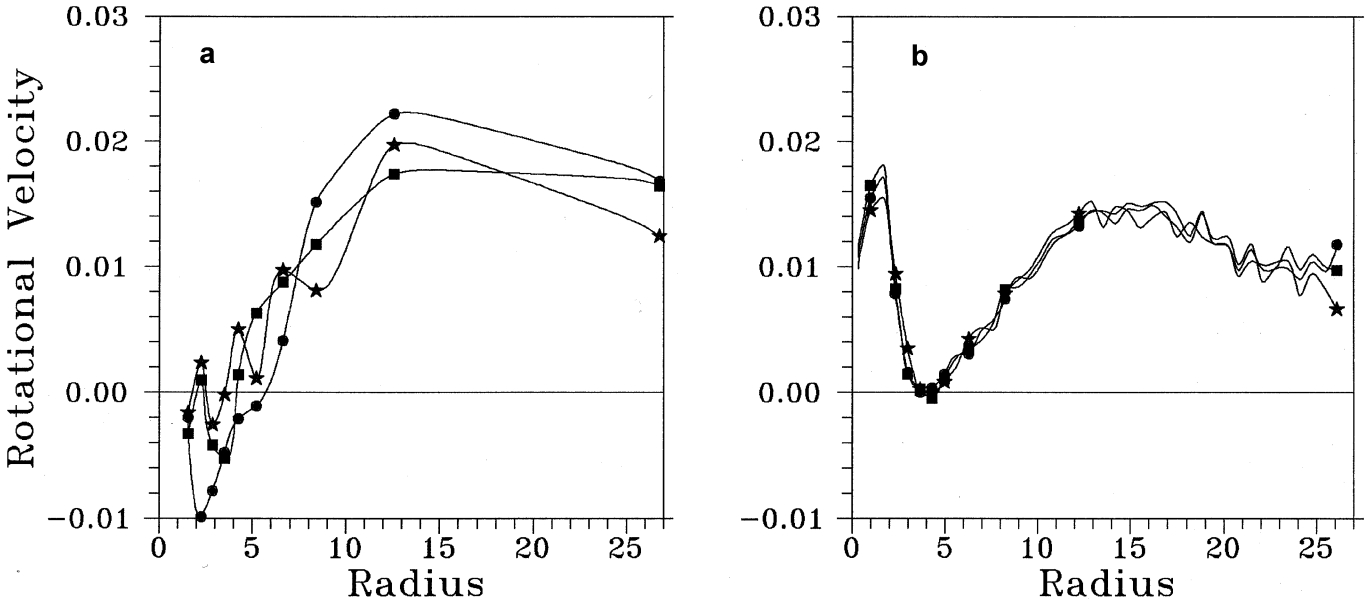

Fig. 15a and b. As in Fig. 13, for the experiment E8-55.

ics.The coefficients of the potential in the series expansion are evaluated from the distribution in space of a relatively large number of particles (of the order of 10^5) at any time step. The time-dependent self-consistent potential obtained in this way is given by analytic expressions, and it has a very low noise level that also gives a very low level of numerical diffusion of orbits in phase space. Particles do not "see" their neighbours and they move only under the global self-consistent gravitational field. Both the global behaviour and the individual orbits can be followed in a very good level of accuracy. The c-t code is suitable for simulating the long time evolution of N-body systems that are close to equilibrium. The transition from one configuration to the other is explained thoroughly in Voglis (1994).

In Fig. 13 we compare the time evolution of the rotation curves given from the N-body code (Fig. 13a) and the c-t code (Fig. 13b) for the experiment E4-55. The rotational velocity V_f at every mass fraction f is evaluated as in Fig. 8 but now the values of V_f are the time averages in the intervals $\Delta t_1 = (4000, 8000)$ (curve with stars), $\Delta t_2 = (8000, 12000)$ (curve with squares) and $\Delta t_3 = (12000, 16000)$ (curve with cycles), respectively. This figure shows that the rotation curves from the two codes have only small differences. Therefore, for this experiment our results are reliable for a time comparable to a Hubble time.

In Figs. 14a, b (which are analogous to Figs. 13a, b, but for E5-55, the results from the two codes have again small differ-

ences. The conclusion here is that counterrotation caused from cosmological initial conditions can survive for a Hubble time.

The results from the two codes in the case E8-55 are shown in Figs. 15a, b derived in a similar way as Figs. 13a, b. The two rotational velocity curves are quite different in the inner parts of the system. The rotational velocity in Fig. 15a shows in the inner parts a gradual evolution towards negative values (compare the relative position of stars, squares and circles). Such an evolution does not appear in the c-t run (Fig. 15b). Therefore in this experiment the rotational velocity curve derived by the N-body run is not reliable for times greater than 6000. This is the time scale required for a particle entering a dense cloud to lose its energy by the process of two body relaxation so that finally it is trapped in the cloud. If a galaxy is formed by dissipationless collapse from initial conditions as those of the experiment E8-55, its rotational velocity curve today should resemble that of Fig. 15b.

6. Conclusion

We propose a mechanism by which counterrotating galaxies can be formed by dissipationless collapse directly from cosmological initial conditions (slightly perturbed Hubble flow in the early Universe). This can be considered as an alternative scenario to other processes proposed in the literature. The advantage to the present process is that only simple initial conditions are required specified by a low dimensional space of parameters.

A central bar-like initial density perturbation oriented at an angle $\theta \neq 0^o, 90^o$ with respect to the tidal field of the environment can work as a seed for this effect.

If the major axis of such a bar is comparable to the diameter of a sphere corresponding to one galactic mass, the distribution of angular momentum along the radius in the final object depends on the axial ratio. This ratio can alter the balance between the tightly and loosely bound particles in a galaxy and hence the balance between positive and negative components of angular momentum along the radius. Counterrotation is favored by axial ratios ≈ 0.5.

Acknowledgements. We would like to thank Dr. Sverre Aarseth as well as Drs. Allen, Palmer and Papaloizou for their kind offer of their codes and the useful accompanying instructions. We would also like to thank Professor G. Contopoulos for his helpful comments. This research was supported in part by the General Secreteriat for Research and Technology under PENED grant 293/1995.

References

Allen A.J., Palmer P.L., Papaloizou J., 1990, MNRAS, 242, 576
Barnes J. and Efstathiou G., 1987, ApJ, 319, 575
Barnes, J. and Hernquist, L. 1996, ApJ, 471, 115
Bender R., 1988, A&A, 202, L5
Bender R. Surma P., 1992, A&A, 258, 250
Davies R., Efstathiou G., Fall M., Illingworth G. And Schechter P., 1983 ApJ, 266, 41
Doroshkevich, A.G. 1970, Astrofisika, 6, 581
Franx M., Illingworth G., 1988, Astroph. J., 327, L55
Franx M., Illingworth G., Heckman T., 1989, Astroph., J., 344, 613
Hoyle, F. 1949, "Problems of Cosmical Aerodynamics (Dayton, Ohio) p.195
Hernquist L., Barnes J.,1991, Nature, 354, 210
Peebles P.J.E., 1969, Astroph. J., 155, 393
Quinn P.J., Salmon J.K., Zureck, W.H., 1986, Nature, 322, 329
Thakar A.R., and Ryden B.S., 1996, Astrophys.J., 461, 55
Voglis N., Hiotelis N., 1989, A&A, 218, 1
Voglis N., Hiotelis N. and Hoflich P., 1991 A&A, 249, 5
Voglis N., 1994, MNRAS, 267, 379
White S.D.M., 1984, Astroph. J., 286, 38
Zeldovich Ya.B., 1970, Astro. Astrophys., 5, 84